

## A 1.75 mm PERIOD RF-DRIVEN UNDULATOR\*

F. Toufexis<sup>†1</sup>, S.G. Tantawi, SLAC, Menlo Park, CA 94025

<sup>1</sup>Also at Department of Electrical Engineering, Stanford University, Stanford, CA 94305.

### Abstract

To reduce the linac energy, and hence the size required for a Free Electron Laser radiating at a given wavelength, a smaller undulator period with sufficient field strength is needed. Previous work from our group successfully demonstrated a microwave undulator at 11.424 GHz using a corrugated cylindrical waveguide operating in the  $HE_{11}$  mode. Scaling down the undulator period using this technology poses the challenge of confining and coupling the electromagnetic fields while maintaining over-moded features for power handling capability and electron beam wakefield mitigation. In this work, we present a novel end section of an RF undulator at 91.392 GHz. To confine the fields inside the undulator, a corrugated waveguide is connected through a matching section to a linear taper and a mirror. After the mirror, a Bragg reflector and a matching section are used to reflect back all the fields leaking out of the mirror opening.

### INTRODUCTION

Free-Electron Lasers (FELs) are tunable sources of high-power, coherent electromagnetic radiation from microwave frequencies all the way to hard X-rays. In biology and material science, SLAC's Linac Coherent Light Source (LCLS) [1] – the first operational hard X-ray FEL – has revealed the structure of key biomolecules [2] and catalysts and their interactions [3]. However, hard X-Ray FELs are very large and expensive. The European XFEL is 2.1 km long, and will generate 0.1 nm photons once completed. It is expected to cost €1.1B, while operational expenses are estimated at €83M/year [4]. Developing a technology that reduces the size and cost of FELs, and makes them accessible to more scientists, will have tremendous impact in advancing science.

Traditionally, coherent emission of short wavelength electromagnetic radiation employed undulators – devices that generate a periodic magnetic field – made of permanent magnets. Such undulators present several limitations on how short their period can be while maintaining reasonable field strength and beam aperture. In order to shrink an FEL, a smaller linac, and therefore lower beam energy, is required. This means that a smaller undulator period is required while sufficient field strength is maintained. However, the undulator wavelength cannot be too small – for example using directly a laser beam [5, 6] – because the emittance requirements make it infeasible for the beam to lase. Alternatives to traditional undulators are in-vacuum and superconducting magnet-based undulators [7–9], crystalline undulators

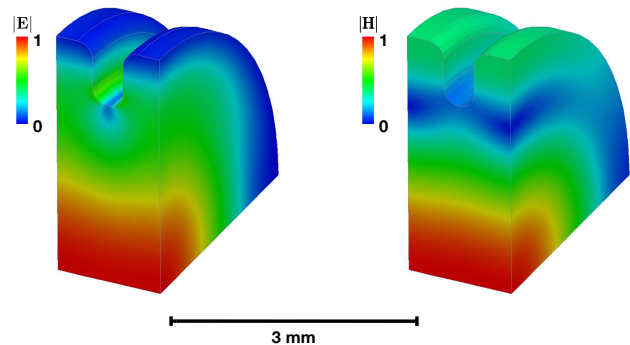


Figure 1: Surface electric and magnetic field of a corrugated waveguide unit cell.

[10, 11], short-period electromagnet-based undulators [12], microfabricated permanent magnet undulators [13], microfabricated electromagnet undulators [14, 15], laser-driven undulators [16–19], and microwave undulators [20, 21]. In-vacuum undulators, short-period electromagnet-based undulators, microfabricated permanent magnet undulators and microfabricated electromagnet undulators are all limited by the beam aperture being smaller than their period in order to maintain high fields. Laser-driven undulators are also limited by small beam apertures. Superconducting undulators are very expensive and present several reliability issues in high-energy beams. Crystalline undulators are still in their infancy and are not suitable for high-current beams. Previous work in our group on microwave undulators investigated several overmoded waveguide systems [22, 23] and concluded that corrugated cylindrical waveguides operating in the  $HE_{11}$  mode were superior in terms of peak field and resistive losses. Such an undulator has been successfully demonstrated at 11.424 GHz [21]. Scaling this undulator into the mm-wave/terahertz regime could dramatically reduce the size and cost of an FEL.

In this work we report the design for a microwave-driven undulator at 91.392 GHz. The end sections have been significantly modified from [21] in order to present large beam apertures. In these end sections, a corrugated waveguide is connected through a matching section to a linear taper and a mirror. After the mirror, a Bragg reflector and a matching section are used to reflect back all the fields leaking out of the mirror opening. Power is coupled into this undulator through the beam pipe by a cylindrical  $TE_{11}$  mode. We have also designed a mode converter from a Gaussian beam to cylindrical  $TE_{11}$ , which is reported in [24].

\* This project was funded by U.S. Department of Energy under Contract No. DE-AC02-76SF00515, and the National Science Foundation under Contract No. PHY-1415437.

<sup>†</sup> ftouf@stanford.edu

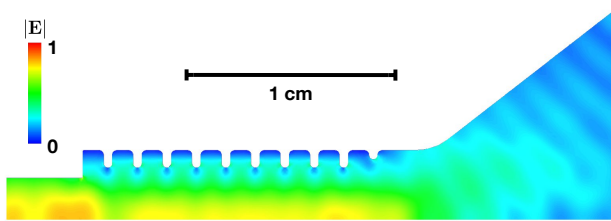
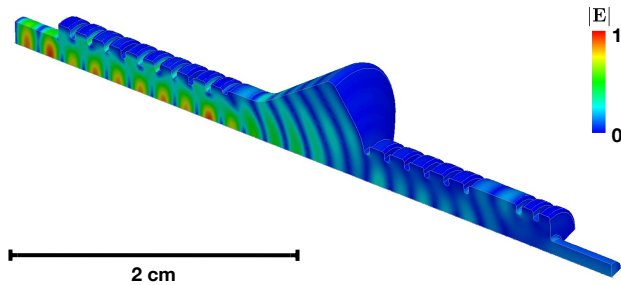
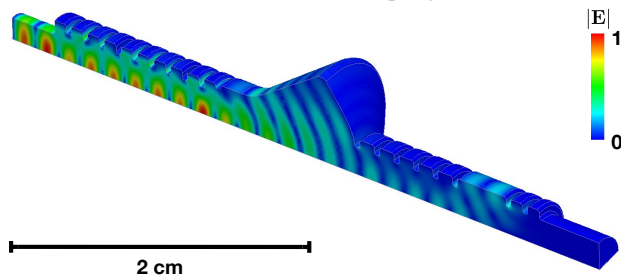


Figure 2: Surface electric field of the linear taper.



(a) Surface electric field of the Coupling End Section.



(b) Surface electric field of the Reflecting End Section.

Figure 3: End section designs.

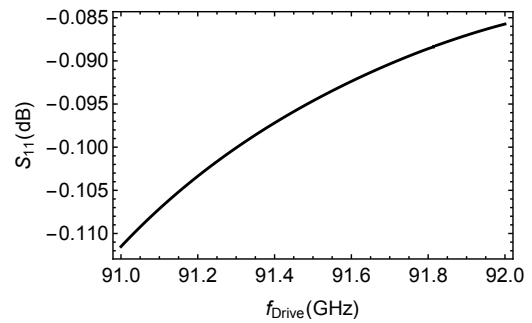
## UNDULATOR DESIGN

### Corrugated WG Single Period

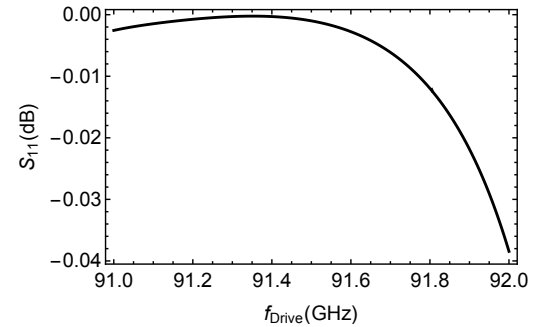
The corrugated waveguide dimensions of the body of the undulator are based on scaling [21]. The thickness of the irises of the corrugated waveguide has been doubled from [21]. The irises are now approximately 400  $\mu\text{m}$  thick and are fully rounded for manufacturability. Figure 1 shows the unit cell of the corrugated waveguide that forms the body of the undulator. The quality factor is 24,732, and the phase advance per unit cell is 134.3°.

### End-Section Design

A cylindrical waveguide  $\text{TE}_{11}$  to corrugated waveguide  $\text{HE}_{11}$  transition is used to launch  $\text{HE}_{11}$  inside the corrugated waveguide. A linear taper with a smooth edge is added. The radius of the smooth edge and the angle of the taper are optimized to minimize reflected power. The inner radius of the last iris of the corrugated waveguide before the linear taper is increased to reduce the peak field in the final cavity. By modifying this feature the peak electric field in the undulator cavity is reduced by approximately 30%. Figure 2 shows a simulation of the linear taper with the corrugated waveguide. Using the field results of this simulation, a mirror is fitted



(a) Reflection coefficient of the Coupling End Section.



(b) Reflection coefficient of the Reflecting End Section.

Figure 4: End section reflection coefficient.

at the end of the taper. The mirror is a metallic surface that is fitted in such a way that is perpendicular to the Poynting vector of the field, and therefore perfectly reflects an electromagnetic wave. Algorithm 1 calculates the surface of the mirror. The collection of points obtained with this procedure constitutes the surface of the mirror. Once the mirror surface is calculated, a hole is created that has the same radius as the inner radius of the corrugated waveguide. The point where the mirror connects to the linear taper is further smoothed, in order to avoid field enhancement. Note that this is a surface with unique geometry that cannot be fitted in a standard shape like an ellipse; otherwise the wave will not be reflected with the correct phase to launch the desired mode in the waveguide. After the mirror, five periods of a Bragg reflector are used to reflect most of the field that leaked from the mirror. The Bragg reflector is a corrugated waveguide, similar to the body of the undulator, but has a period of exactly half a wavelength. The field in a Bragg reflector is exponentially decaying. The Bragg reflector cannot be used to perfectly reflect power because for it to do so would require too many periods and increase the size and losses of the overall device. Instead, two more corrugated periods, spaced with a smooth wall waveguide from the Bragg reflector are used to reflect the remaining power. The length of this smooth walled cylindrical waveguide controls the amount of RF power leaked from the end section.

We have designed two different end sections for the two sides of the undulator, shown in Fig. 3. One end section is placed on the side of the undulator that interfaces with the

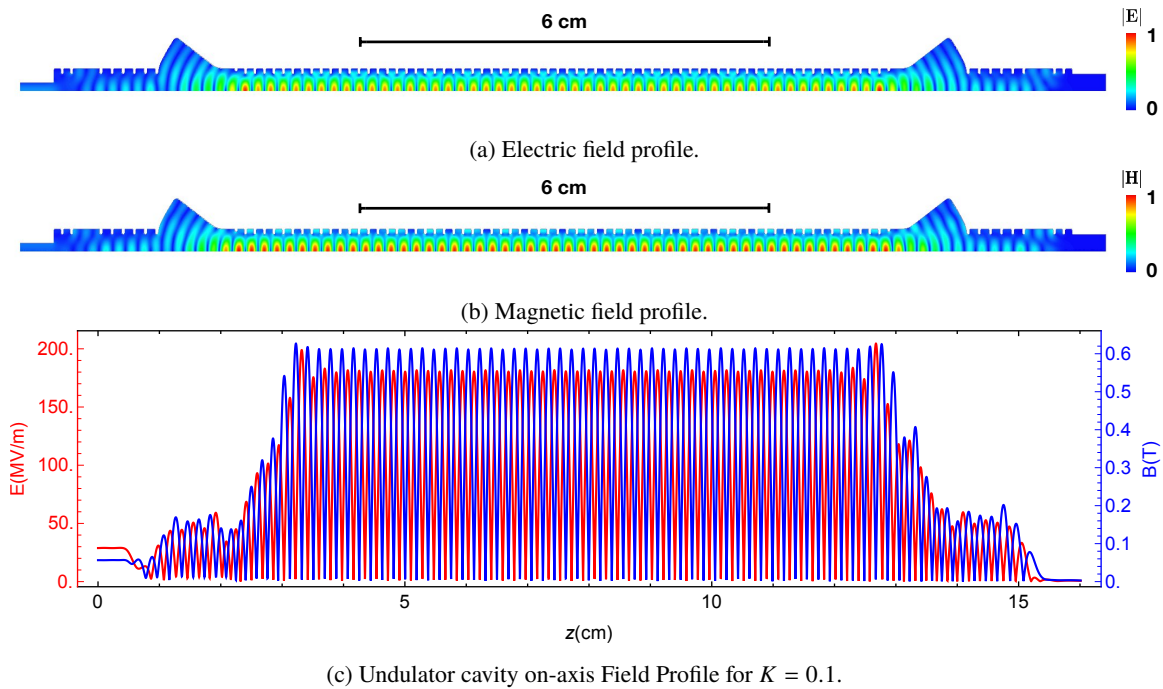


Figure 5: Undulator Cavity.

**Data:** Field profile

**Result:** List of mirror points

Start at a point on-axis at the end of the linear taper;

**while** wall of the linear taper is not reached **do**

    Calculate the Poynting vector at the current point

$$\mathbf{S} = \frac{1}{2} \mathbf{E} \times \mathbf{H};$$

    Calculate the vector  $\mathbf{P}$  perpendicular to  $\mathbf{S}$ , towards positive  $r$ ;

    Calculate a point along  $\mathbf{P}$  that is a small fraction of wavelength away from the current point;

    Save the new point in list of mirror points;

**end**

**Algorithm 1:** Mirror Fitting Algorithm.

Gaussian to  $TE_{11}$  mode converter. This end section connects to the cylindrical waveguide of the mode converter and is designed to leak approximately  $-16.5$  dB of power inside the cylindrical waveguide. This amount of power corresponds to the undulator cavity being critically coupled. The second end section is connected to a beam pipe with the same radius as the inner radius of the corrugated waveguide and is designed to be perfectly reflecting. By making the output beam pipe of the second end section as big as possible, we anticipate to leak any parasitic modes excited by the beam.

This design of the end sections has the advantage of having a large aperture for the beam  $-2.375$  mm  $-$  while being broadband. The resonance frequency of the mode of interest is mainly affected by the mirrors. Manufacturing imperfections in the position of the mirrors, which would cause a shift in resonance frequency, can be compensated for by using thermal tuning. As shown in Fig. 4, the reflection coefficient

of both end sections varies very little with frequency across  $0.5$  GHz. We believe this is an indication that the coupling of the design (which is affected by the end sections) will be relatively insensitive to manufacturing imperfections.

### Undulator Cavity

Figure 5 shows the entire undulator cavity. The intrinsic quality factor is  $25,235$ , and the total quality factor is  $12,707$ . Figure 5c shows the field profile on the axis of the undulator. This figure shows that the field profile is flat inside the undulator, and smoothly tapers at the end section, without major spikes that could kick the beam. The undulator period is  $1.75$  mm. The RF power required for  $K = 0.1$  is  $1.4$  MW. The corresponding peak electric and magnetic fields on the metallic surface are  $107$  MV  $m^{-1}$  and  $269$  kA  $m^{-1}$ . From [25] the peak pulsed surface heating for  $250$  ns RF pulses is  $44$  °C, which is considered safe for copper [26].

## CONCLUSION

We reported the design of a short-period microwave driven undulator at  $91.392$  GHz. The undulator period is  $1.75$  mm and the beam aperture diameter is  $2.375$  mm. The required power for  $K = 0.1$  is  $1.4$  MW, and the undulator can operate at that power level for  $250$  ns for copper. Power is coupled to the undulator through the beam pipe carrying  $TE_{11}$ .

## REFERENCES

- [1] P. Emma *et al.*, "First lasing and operation of an ångstrom-wavelength free-electron laser," *Nature Photonics*, vol. 4, no. 9, pp. 641–647, Aug. 2010.

- [2] G. Fenalti *et al.*, “Structural basis for bifunctional peptide recognition at human  $\delta$ -opioid receptor,” vol. 22, no. 3, pp. 265–268.
- [3] J. Kern *et al.*, “Simultaneous Femtosecond X-ray Spectroscopy and Diffraction of Photosystem II at Room Temperature,” *Science*, vol. 340, no. 6131, pp. 491–495, 2013.
- [4] M. Altarelli *et al.*, “The European X-Ray Free Electron Laser: Technical design report,” Tech. Rep., Jul. 2007.
- [5] R. J. Loewen, “A Compact Light Source: Design and Technical Feasibility Study of a Laser-Electron Storage Ring X-Ray Source,” Ph.D. dissertation, Stanford University, 2003.
- [6] W. S. Graves *et al.*, “Compact x-ray source based on burst-mode inverse Compton scattering at 100 kHz,” *Phys. Rev. ST Accel. Beams*, vol. 17, no. 12, p. 120701, Dec. 2014.
- [7] T. Tanaka *et al.*, “In-vacuum undulators,” in *Proceedings of the 27th International Free Electron Conference*, 2005, pp. 370–377.
- [8] J. Bahrtdt and Y. Ivanyushenkov, “Short Period Undulators for Storage Rings and Free Electron Lasers,” *Journal of Physics: Conference Series*, vol. 425, no. 3, p. 032001, 2013.
- [9] Y. Ivanyushenkov *et al.*, “Development of a superconducting undulator for the APS,” *Journal of Physics: Conference Series*, vol. 425, no. 3, p. 032007, 2013.
- [10] S. Bellucci *et al.*, “Experimental Study for the Feasibility of a Crystalline Undulator,” *Phys. Rev. Lett.*, vol. 90, no. 3, p. 034801, Jan. 2003.
- [11] E. Bagli *et al.*, “Experimental evidence of planar channeling in a periodically bent crystal,” *The European Physical Journal C*, vol. 74, no. 10, p. 3114, 2014.
- [12] S. Yamamoto, “A novel attempt to develop very short period undulators,” *Journal of Physics: Conference Series*, vol. 425, no. 3, p. 032014, 2013.
- [13] B. A. Peterson *et al.*, “Technology Development for Short-period Magnetic Undulators,” *Physics Procedia*, vol. 52, pp. 36–45, 2014.
- [14] J. Harrison *et al.*, “Surface-micromachined magnetic undulator with period length between 10  $\mu\text{m}$  and 1 mm for advanced light sources,” *Phys. Rev. ST Accel. Beams*, vol. 15, no. 7, p. 070703, Jul. 2012.
- [15] J. Harrison *et al.*, “Surface-micromachined Electromagnets for 100 $\mu\text{m}$ -scale Undulators and Focusing Optics,” *Physics Procedia*, vol. 52, pp. 19–26, 2014.
- [16] T. Plettner and R. L. Byer, “Proposed dielectric-based microstructure laser-driven undulator,” *Phys. Rev. ST Accel. Beams*, vol. 11, no. 3, p. 030704, Mar. 2008.
- [17] A. D. Debus *et al.*, “Traveling-wave Thomson scattering and optical undulators for high-yield EUV and X-ray sources,” *Applied Physics B*, vol. 100, no. 1, pp. 61–76, 2010.
- [18] V. Karagodsky and L. Schächter, “High efficiency x-ray source based on inverse Compton scattering in an optical Bragg structure,” *Plasma Physics and Controlled Fusion*, vol. 53, no. 1, p. 014007, 2011.
- [19] F. Toufexis, T. Tang, and S. G. Tantawi, “A 200  $\mu\text{m}$ -period Laser-Driven Undulator,” in *Proc. of the Free-Electron Laser Conference, Basel, Switzerland, Aug. 2014*. JACoW, 2014.
- [20] T. Shintake, “Experimental Results Of Microwave Undulator,” *International Conference on Insertion Devices for Synchrotron Sources*, vol. 0582, pp. 336–343, May 1986.
- [21] S. Tantawi *et al.*, “Experimental Demonstration of a Tunable Microwave Undulator,” *Phys. Rev. Lett.*, vol. 112, no. 16, p. 164802, Apr. 2014.
- [22] S. Tantawi *et al.*, “A coherent Compton backscattering high gain FEL using an X-band microwave undulator,” *FEL*, 2005.
- [23] M. Shumail *et al.*, “Application of the Balanced Hybrid Mode in Overmoded Corrugated Waveguides to Short Wavelength Dynamic Undulators,” *Conf. Proc.*, vol. C110904, pp. 3328–3330, 2011.
- [24] F. Toufexis, J. Neilson, and S. G. Tantawi, “Coupling and Polarization Control in a mm-wave Undulator,” in *Proc. of International Particle Accelerator Conference (IPAC'17), Copenhagen, Denmark, May 14-19, 2017*. Geneva, Switzerland: JACoW, May 2017.
- [25] V. A. Dolgashev, “High magnetic fields in couplers of X-band accelerating structures,” in *Proceedings of the 2003 Particle Accelerator Conference*, May 2003, pp. 1267–1269 Vol.2.
- [26] L. Laurent *et al.*, “Experimental study of rf pulsed heating,” *Phys. Rev. ST Accel. Beams*, vol. 14, no. 4, p. 041001, Apr. 2011.